Regularity in chaotic reaction paths. I. Ar_6

Tamiki Komatsuzaki[a] and R. Stephen Berry
Department of Chemistry, The University of Chicago, Chicago, Illinois 60637

(Received 27 October 1998; accepted 16 February 1999)

We scrutinize the saddle crossings of a simple cluster of six atoms to show (a) that it is possible to choose a coordinate system in which the transmission coefficient for the classical reaction path is unity at all energies up to a moderately high energy, above which the transition state is chaotic; (b) that at energies just more than sufficient to allow passage across the saddle, all or almost all the degrees of freedom of the system are essentially regular in the region of the transition state; and (c) that the degree of freedom associated with the reaction coordinate remains essentially regular through the region of the transition state, even to moderately high energies. Microcanonical molecular dynamics simulation of Ar_6 bound by pairwise Lennard-Jones potentials reveals the mechanics of passage. We use Lie canonical perturbation theory to construct the nonlinear transformation to a hyperbolic coordinate system which reveals these regularities. This transform ''rotates away'' the recrossings and nonregular behavior, especially of the motion along the reaction coordinate, leaving a coordinate and a corresponding dividing surface in phase space which minimize recrossings and mode–mode mixing in the transition state region. The action associated with the reactive mode tends to be an approximate invariant of motion through the saddle crossings throughout a relatively wide range of energy. Only at very low energies just above the saddle could any other approximate invariants of motion be found for the other, nonreactive modes. No such local invariants appeared at energies at which the modes are all chaotic and coupled to one another. [S0021-9606(99)50918-5]

I. INTRODUCTION

Several recent studies of Hamiltonian systems have focused on the characterization of dynamical properties in terms of the Liapunov exponents, Kolmogorov entropy (K entropy), and related indices, especially to relate these to the topologies and topographies of the corresponding potential energy surfaces (PESs).[1–5] These investigations have provided us with several new insights into the molecular foundations of chemical reactions. Berry and co-workers have used the isomerization of clusters to explore the nonuniformity of dynamical properties insofar as they depend on the local character and topography of the potential energy surfaces. Amitrano and Berry[1] have found how the largest local Liapunov exponents of Ar_3 reveal that the motion in the linear saddle region of this simple system is more regular than that in the potential well around the equilateral minimum, near the temperature at which the system can just cross the saddle, even though the dynamics in the potential well is fully chaotic under these conditions.[2] By analyzing local K entropies and other related measures, Hinde and Berry[3] clarified how, in small inert gas clusters (the number of atoms $N=3-5$), the flat saddles effectively regularize the cluster dynamics close to the saddle point and how such saddles in some cases can decouple some or all of the cluster's vibrational modes from one another. This decoupling leads to the occurrence of local or regional quasiconstant action variables in the saddle regions. Their analyses were carried out by dividing the trajectories into segments corresponding to motions in the bowls around the local potential minima, motion in the saddle regions, and motion in transition regions between local wells and saddles. These regions were assigned according to the quenched energies in the centers of the trajectory segments. They also analyzed some larger inert gas clusters ($N=6,7$), but the possibility of inference of regular regions by the method they used seemed to be limited to small clusters ($N=3-5$). At that time, there was no general method apparent by which an optimal coordinate transformation could be found to allow one to infer the extent of constancy of the action in a single degree of freedom (DOF) along a chosen segment of a reaction path, especially in the region of a transition state. This meant that it seemed very difficult to examine larger complex systems to extract from the full space of the vibrational DOF a coordinate, if such exists, that would exhibit whatever regularized or less-chaotic dynamics might occur in transition states. In other words, this meant that it seemed very difficult to determine the extent to which the reaction coordinate becomes decoupled from other modes of internal motion as the system passes through its reaction bottleneck.

The recent remarkable experimental study by Lovejoy *et al.*[6] of unimolecular dissociation of highly vibrationally excited ketene, with nine internal DOF, revealed that the rate of this reaction is controlled by the flux through quantized thresholds in the transition state. As stated by Marcus,[7] this behavior indicates that the transverse vibrational quantum numbers might indeed be approximate constants of motion.

Ohmine and co-workers[8] have shown that the power spectra of liquid water dynamics yield a clear $1/f$-noise

[a]Visiting researcher from Institute for Fundamental Chemistry, 34-4 Takano-Nishihirakicho, Sakyo-ku, Kyoto 606 Japan (–March 1998).

structure and the dynamics consists of chaotic vibrational motions around each minimum energy configuration, with slower transitions among the configurations. These transitions occur intermittently, not as simple thermal random motions of individual molecules, but as cooperative dynamical processes with collective molecular motions. The results suggest that the transition through its reaction bottleneck in water is less chaotic than the motions around potential minima, similar to the behavior of small clusters. If the system were entirely stochastic, it would be improbable that one could identify specific modes of cooperative motion. The studies of such large, many-DOF systems suggest that at typical energies at which isomerizations occur, such systems do not exhibit ''fully developed'' chaos. That is, some approximate or ''vague''[9] invariant manifolds may well exist in some parts of the phase space whose dimensions are less than the system's full degrees of freedom, and suppress a fast evolution of chaos for some specific DOF.

The need to introduce transmission coefficients less than 1 is a well-known *ad hoc* fixture of classical transition state theory. Davis and Gray[10] first showed that in Hamiltonian systems with only two DOF, the transition state defined as the separatrix in the phase space is always free from barrier recrossings, so the transmission coefficient for such systems is unity. Their inference depends crucially on the Poincaré section having only two dimensions; no general theory exists yet for systems of higher dimensionality.[11–14]

Recently Komatsuzaki *et al.*[15,16] developed a new method to examine the regularity of multidimensional saddle crossings, based on Lie canonical perturbation theory (LCPT), which most effectively provides us with a classical footing of regularity of the nonlinear dynamics of the system. They showed that the saddle-crossing dynamics of a four-DOF Hamiltonian, a model of proton transfer in malonaldehyde, is interpretable as fully quasiperiodic (i.e., the system has four approximate constants of motion), and the recrossing motions transform into no-return crossing motions over a new dividing surface in the phase space. One might expect that the greater the number of DOF, the more frequently (near-) resonance conditions would occur in the phase space, and that these would generate mode–mode mixing that would spoil approximate invariants of motion. A major point of this work is to show that *local* approximate invariants may persist even to moderately high energies, specifically in the regions of transition states. To do this, we have had to address the problem of extracting a ''general'' dividing surface as free as possible from recrossings; to extend this to arbitrarily high energies at which the saddle crossings are chaotic, for multidimensional systems, is still an unsolved and perhaps unsolvable problem.

We consider two fundamental questions throughout this paper.

(1) How do the topological features of a potential surface transform the dynamics of saddle crossings as the energy of the reacting system increases from threshold to much higher values? As a corollary, what role do saddles, including those of rank higher than 1, play in the system's transition from regular to chaotic dynamics?

(2) In the context of reaction dynamics, how can we extract a dividing surface as free as possible from recrossings between the reactant and product states?

The outline of this paper is as follows. In Sec. II, we review our method and technique, the algebraic quantization by LCPT for a regional Hamiltonian about any stationary point. In Sec. III, we describe the model and the details of calculations. In Sec. IV, we present our results and discussion. Finally, we give some concluding remarks in Sec. V. A brief account of this work has been prepared.[17]

II. THEORY

A. Lie canonical perturbation theory

We begin by reviewing Lie canonical perturbation theory (LCPT) and the physical implications. Canonical perturbation theories[18] transform $(\mathbf{p},\mathbf{q})$ to a new $(\overline{\mathbf{p}},\overline{\mathbf{q}})$ coordinate system so as to make the new Hamiltonian $\overline{H}(\overline{\mathbf{p}},\overline{\mathbf{q}})$ as close to integrable as possible. The traditional approach, based on mixed-variable generating functions F;

$$\overline{\mathbf{q}}=\frac{\partial F(\overline{\mathbf{p}},\mathbf{q})}{\partial\overline{\mathbf{p}}},\quad \mathbf{p}=\frac{\partial F(\overline{\mathbf{p}},\mathbf{q})}{\partial\mathbf{q}} \tag{1}$$

requires functional inversion to obtain explicit formulas for $(\mathbf{p},\mathbf{q})$ in terms of $(\overline{\mathbf{p}},\overline{\mathbf{q}})$ and vice versa, at each order of the perturbative calculation, which imposes a major difficulty to implementing higher-order perturbations and to treating many-degrees-of-freedom systems. Lie canonical perturbation theories (LCPTs)[15,16,18–25] are superior to the traditional methods, in that no cumbersome functions of mixed variables appear and all the terms in the series are repeating Poisson brackets. The LCPT is based on Lie transforms, that is, the exponential of a Lie operator induces a canonical transformation: Let L_w be the Lie operator associated with a generating function w,

$$L_w\equiv\{w,\} \tag{2}$$

where $\{\}$ denotes the Poisson bracket. Then the transformation of an autonomous Hamiltonian H to a new Hamiltonian $\overline{H}$,

$$H(\mathbf{p},\mathbf{q})\rightarrow\overline{H}(\overline{\mathbf{p}},\overline{\mathbf{q}})=\exp(L_w)H(\overline{\mathbf{p}},\overline{\mathbf{q}}), \tag{3}$$

is canonical. We let H be an M-dimensional Hamiltonian expandable in ϵ (=strength of the perturbation) where the zeroth-order Hamiltonian H_0 is assumed to be integrable, e.g., a system of M harmonic oscillators. Such a system is a function of action variables $\mathbf{J}$ only, and does not depend on the conjugate angle variables $\mathbf{\Theta}$,

$$H(\mathbf{p},\mathbf{q})=\sum_{n=0}\epsilon^n H_n(\mathbf{p},\mathbf{q}) \tag{4}$$

$$=H_0(\mathbf{J})+\sum_{n=1}\epsilon^n H_n(\mathbf{J},\mathbf{\Theta}) \tag{5}$$

$$=\sum_{k=1}^{M}\omega_k J_k+\sum_{n=1}\epsilon^n H_n(\mathbf{J},\mathbf{\Theta}), \tag{6}$$

where ω_k is the fundamental frequency of the kth mode. Assuming the new Hamiltonian $\bar{H}$ and the generating function w are also expandable in ϵ, we substitute all H, $\bar{H}$, and w to Eq. 3 and determine the new Hamiltonian, at each order in ϵ, to be as a simple a form as possible by eliminating, as much as possible, its dependencies on the new angle variables $\bar{\boldsymbol{\Theta}}$.[15,18,20] If the $\bar{H}$ is obtained free from the angle $\bar{\boldsymbol{\Theta}}$ (at the order of the perturbative calculation performed):

$$\bar{H}(\bar{\mathbf{p}},\bar{\mathbf{q}})=\bar{H}(\bar{\mathbf{J}},\bar{\boldsymbol{\Theta}})=\bar{H}(\bar{\mathbf{J}})=\sum_{n=0}\epsilon^n\bar{H}_n(\bar{\mathbf{J}}), \tag{7}$$

the new action and angle variables for the kth mode are expressed as

$$\frac{d\bar{J}_k}{dt}=\dot{\bar{J}}_k=-\frac{\partial\bar{H}(\bar{\mathbf{J}})}{\partial\bar{\Theta}_k}=0, \tag{8}$$

$$\bar{J}_k=\text{constant}\quad (k=1,2,3,\ldots,M), \tag{9}$$

and

$$\dot{\bar{\Theta}}_k=\frac{\partial\bar{H}(\bar{\mathbf{J}})}{\partial\bar{J}_k}\equiv\bar{\omega}_k(\bar{\mathbf{J}})=\text{constant}, \tag{10}$$

$$\bar{\Theta}_k=\bar{\omega}_k(\bar{\mathbf{J}})t+\beta_k, \tag{11}$$

where β_k is the arbitrary initial phase factor of the kth mode. From there, the equations of motion with respect to the new coordinates $\bar{\mathbf{q}}$ and momenta $\bar{\mathbf{p}}$ are obtained from the Hamiltonian equations of motion obeying $\bar{H}$;

$$\frac{d^2\bar{q}_k(\mathbf{p},\mathbf{q})}{dt^2}+\bar{\omega}_k^2\bar{q}_k(\mathbf{p},\mathbf{q})=0, \tag{12}$$

and

$$\bar{p}_k(\mathbf{p},\mathbf{q})=\frac{\omega_k}{\bar{\omega}_k}\frac{d\bar{q}_k(\mathbf{p},\mathbf{q})}{dt}, \tag{13}$$

where $\bar{\omega}_k(=\bar{\omega}_k(\bar{\mathbf{J}})=\bar{\omega}_k(\bar{\mathbf{p}},\bar{\mathbf{q}}))$ is independent of time t because the $\bar{\mathbf{J}}$ are constant through all t [Eq. (8)]. Equations (12) and (13) tell us that even though the motions look quite complicated in the old coordinate system, they can be reformulated as simple decoupled periodic orbits in the phase space *if M invariants of motion exist*. In the cases that the M approximate invariants of motion exist in a global (or at least local) region and only in such cases, LCPT provides an analytical solution of the M-dimensional (regional) dynamics, and $\bar{q}_k(\mathbf{p},\mathbf{q})$ and $\bar{p}_k(\mathbf{p},\mathbf{q})$ can actually be decoupled from one another, although they are of course functions of the coupled $\mathbf{p}$ and $\mathbf{q}$ obeying the original system Hamiltonian H. In the following treatment, we seek only canonical transformations whose reductions to action-angle variables are valid in a limited region near a saddle point. We have no expectation of finding that such a transformation would be applicable globally.

The (near-)commensurable conditions that an integer linear combination of fundamental frequencies vanishes identically at a given order ϵ^n,

$$\sum_{k=1}^{M}n_k\omega_k\leqslant O(\epsilon^n) \tag{14}$$

(n_k is arbitrary integer), make the corresponding new Hamiltonian, Eq. (7), diverge ultimately and destroy invariants of motion.[18] If the system exhibits near-commensurable conditions, the new Hamiltonian probably cannot be represented as a function of constant (or near-constant) actions only; instead the perturbative calculation would have to be performed to infinite order, or the new Hamiltonian would include the corresponding angle variables to avoid divergence.[23–25]

It is likely in many M-dimensional systems that the near-commensurable conditions densely distribute in the phase space, i.e., the occupation ratio of the M-dimensional tori in the phase space is negligibly small. However, it may be anticipated that in some many-dimensional systems, e.g., clusters, water, and biological systems, except at very high energies, some but not all of the approximate constants survive so that in some region or regions, an approximate, or ''vague'' invariant manifold exists with dimension less than M. Otherwise, one could hardly understand the reason why nonrandom, collective atomic/molecular motions are observed there. In such cases, LCPT is still powerful enough to reveal such an invariant manifold; this and its implications are the main subject we explore in this paper.

B. The regional Hamiltonian

Despite its versatility, LCPT has not been applied to many-DOF realistic atomic/molecular systems. One of the two main difficulties is how one could handle the analytical derivative and integral calculations that appear successively in the LCPT procedure. The other is the near impossibility of obtaining even moderately simple analytical expressions to describe the accurate (e.g., *ab initio*) potential energy surfaces (PESs) in full. The dynamical properties of multidimensional Hamiltonian systems are revealed to be strongly nonuniform, depending on the local topography of their PESs.[1,3] In such cases, except at very high energies, a versatile procedure is one of focusing on the *regional* dynamical properties by dividing the time series of trajectories into time segments[1] or by dividing PESs into cells, e.g., minima, saddle,... and examining these.[3] We propose an efficient LCPT method, of the latter type, which enables us to analyze local regularity in dynamics in the vicinity of an arbitrary stationary point.[15,16]

We first expand the full $3N$-DOF potential energy surface about a chosen stationary point, i.e., minimum, saddle, or higher-rank saddle. By taking the zeroth-order Hamiltonian as a harmonic oscillator system, which might include some negatively curved modes, i.e., reactive modes, we establish the higher-order perturbation terms to consist of nonlinear couplings expressed in arbitrary combinations of coordinates,

$$H=H_0+\sum_{n=1}^{\infty}\epsilon^nH_n, \tag{15}$$

where

$$H_0=\frac{1}{2}\sum_j (p_j^2+\omega_j^2 q_j^2), \tag{16}$$

$$\sum_{n=1}^{\infty}\epsilon^n H_n=\epsilon\sum_{j,k,l} C_{jkl}q_j q_k q_l + \epsilon^2\sum_{j,k,l,m} C_{jklm}q_j q_k q_l q_m+\cdots. \tag{17}$$

Here, q_j and p_j are the jth normal coordinate and its conjugate momentum, respectively; ω_j and C_{jkl}, C_{jklm}, ... are, respectively, the frequency of the jth mode, the coupling coefficient among q_j, q_k, and q_l, and that among q_j, q_k, q_l, and q_m and so forth. The frequency associated with an unstable reactive mode F and those of the other stable modes B are pure-imaginary and real, respectively. At any stationary point there are six zero-frequency modes corresponding to the total translational and infinitesimal rotational motions, and the normal coordinates of the infinitesimal rotational motions appear in the perturbation terms $H_n(\mathbf{q})(n>0)$. The contribution of the total translational motion is simply separated. We make no more mention of this. If one deals with a system whose total angular momentum is zero, one could eliminate the contributions of the total rotational motions from $H_n(\mathbf{q})(n>0)$ by operating with a suitable projection operator;[26] at the stationary point it corresponds to putting to zero each normal coordinate and corresponding conjugate momentum representing the infinitesimal total rotational motion.[27] If the total angular momentum is not zero, the coupling elements among the rotational and vibrational modes must be taken into account. For the sake of simplicity we focus on a $(3N\text{-}6)$-DOF Hamiltonian system with total linear and angular momenta of zero, so that the kinetic and potential energies are purely vibrational.[28] For such a zeroth-order Hamiltonian $\omega_k\neq 0$ for all $k(=1,2,3,\ldots,3N-6\ (\equiv M))$, the associated action-angle variables of the stable modes $B(\omega_B\in\Re\text{:real})$ and the unstable mode $F(\omega_F\in\Im\text{:imaginary})$ are expressed as

$$J_B=\frac{1}{2\pi}\oint p_B\,dq_B=\frac{1}{2}\left(\frac{p_B^2}{\omega_B}+\omega_B q_B^2\right), \tag{18}$$

$$\Theta_B=\tan^{-1}\left(\frac{p_B}{\omega_B q_B}\right), \tag{19}$$

and

$$J_F=\frac{1}{2\pi}\mathrm{Im}\int_{\text{barrier}} p_F\,dq_F, \tag{20}$$

$$=\frac{i}{2}\left(\frac{p_F^2}{|\omega_F|}-|\omega_F|q_F^2\right), \tag{21}$$

$$\Theta_F=i\tanh^{-1}\left(\frac{p_F}{|\omega_F|q_F}\right),\quad \omega_F\equiv-|\omega_F|i. \tag{22}$$

Here the action associated with the reaction mode F, having first been postulated in the semiclassical transition state theory,[29–31] is purely imaginary and is connected with the barrier penetration integral in the semiclassical theory. It is easily verified[32] that any set of variables $\mathbf{J}$ and $\mathbf{\Theta}$ is canonical, including those associated with the unbound mode F.

C. The algebraic quantization method

For practical LCPT calculations of the above Hamiltonians, a quite efficient method, called ''algebraic quantization,'' has been developed. Some authors have addressed this topic in detail,[15,23–25] so we only present the key prescription here. This method first transforms $(\mathbf{p},\mathbf{q})$ in Eqs. (15)–(17) to $(\mathbf{a}^*,\mathbf{a})$ by the customary means:

$$a_k^*=\frac{1}{\sqrt{2}}(p_k+i\omega_k q_k),\quad a_k=\frac{1}{\sqrt{2}}(p_k-i\omega_k q_k), \tag{23}$$

which are expressed in terms of the old action variable J_k, the associated frequency ω_k, and time τ obeying Hamiltonian H_0 as

$$a_k^*(\tau)=\sqrt{\omega_k J_k}e^{i\Theta_k}=\sqrt{\omega_k J_k}e^{i(\omega_k\tau+\beta_k)}, \tag{24}$$

$$a_k(\tau)=\sqrt{\omega_k J_k}e^{-i\Theta_k}=\sqrt{\omega_k J_k}e^{-i(\omega_k\tau+\beta_k)}. \tag{25}$$

The cumbersome analytical calculations that appeared in the LCPT calculations are then replaced by symbolic operations with no special mathematical manipulators, thanks to the simple Poisson bracket rules for the $(\mathbf{a}^*,\mathbf{a})$,

$$\{a_j^*,a_k^*\}=\{a_j,a_k\}=0,\quad \{a_j^*,a_k\}=i\omega_k\delta_{jk}, \tag{26}$$

where $\{\}$ and δ denote Poisson bracket and Kronecker delta, respectively. We then substitute Eqs. (23)–(25) into Eq. (15), converting the Hamiltonian from the $(\mathbf{p},\mathbf{q})$ to the $(\mathbf{a}^*,\mathbf{a})$ representation, to obtain simultaneous algebraic equations, which readily yield the desired dynamical quantities with the help of Eq. (26).[15]

Finally, we obtain new transformed physical quantities $\overline{A}$, e.g., new Hamiltonian $\overline{H}$, and new action $\overline{J_k}$, frequency $\overline{\omega_k}$, momentum $\overline{p_k}$, and coordinate $\overline{q_k}$ of the kth mode, in terms of the original $\mathbf{p}$ and $\mathbf{q}$ as

$$\overline{A}=\overline{A}(\mathbf{p},\mathbf{q})=\sum_{n=0}\epsilon^n\overline{A}_n(\mathbf{p},\mathbf{q}). \tag{27}$$

In the present paper, we analyze $\overline{A}$ up to a (finite) ϵ^i order $(i=0,1,2)$:

$$\overline{A}^{i\text{th}}=\overline{A}^{i\text{th}}(\mathbf{p},\mathbf{q})=\sum_{n=0}^{i}\epsilon^n\overline{A}_n(\mathbf{p},\mathbf{q}), \tag{28}$$

where no (near-) commensurable conditions were encountered at these orders during our LCPT procedure.

For example, by monitoring the new action of the kth mode $\overline{J_k}(\mathbf{p},\mathbf{q})$ along molecular dynamics (MD) trajectories obeying equations of motion of the original Hamiltonian $H(\mathbf{p},\mathbf{q})$, we can detect whether the $\overline{q_k}$ mode tends to maintain an invariant of motion. If the $\overline{J_k}(\mathbf{p},\mathbf{q})$ and its associated $\overline{\omega_k}(\mathbf{p},\mathbf{q})$ exhibit near constants of motion through a certain time range, it implies that $\overline{p_k}$ and $\overline{q_k}$ are approximately decoupled from the other modes, and represent the local dynamics analytically.

The $\overline{p_k}(\mathbf{p},\mathbf{q})$ and $\overline{q_k}(\mathbf{p},\mathbf{q})$ have the following forms, respectively,

$$\overline{p_k}(\mathbf{p},\mathbf{q})=\sum_j c_j \mathbf{p}^{2n-1}\mathbf{q}^m, \tag{29}$$

$$\overline{q_k}(\mathbf{p},\mathbf{q})=\sum_j d_j \mathbf{p}^{2n}\mathbf{q}^m, \tag{30}$$

where c_j and d_j denote the coefficient of the jth term, n, $m(\geqslant 0)$ are arbitrary integers, and $\mathbf{q}^m=q_1^{m_1}q_2^{m_2}q_3^{m_3}\cdots q_M^{m_M}(\Sigma_{j=1}^M m_j=m)$, etc. The new $\overline{p_k}(\mathbf{p},\mathbf{q})$ and $\overline{q_k}(\mathbf{p},\mathbf{q})$ maintain time reversibility. The contributions of the original p_k and q_k in $\overline{p_k}^{i\text{th}}(\mathbf{p},\mathbf{q})$ and $\overline{q_k}^{i\text{th}}(\mathbf{p},\mathbf{q})$ are not necessarily large and almost all modes contribute to $\overline{p_k}^{i\text{th}}$ and $\overline{q_k}^{i\text{th}}(\mathbf{p},\mathbf{q})$ for $i\geqslant 1$.

The number of terms appearing in the LCPT calculations increases rapidly with the order one wishes to estimate, and with the number of DOF of the system. The total numbers of terms contributing to $\overline{p_1}^{i\text{th}}$ and $\overline{q_1}^{i\text{th}}$ at saddle I, defined below, of Ar_6 are ~ 50 at first, and ~ 450 at second orders. Explicit expressions for the first- and second-order terms of $\overline{p_1}^{i\text{th}}$ and $\overline{q_1}^{i\text{th}}$ at saddle I are available on-line in supplementary material to this paper.[33]

An efficient and fast storing-extracting-(symbolical) manipulating algorithm for the indices classifying each term is thus highly desired. The present program developed in our laboratory takes less than 1 h when computed with a 120–150 MHz Pentium PC with 32 MBytes memory for the saddle Hamiltonians of Ar_6 (24 phase space dimensions), through the second-order LCPT calculation. As far as we know, this is the first example of a large-DOF system ($M>5$) to be studied by the canonical perturbation theory.

D. Reformulation of transition state theory (TST)

In cases where saddle crossing dynamics has approximate invariants of motion associated locally with the reactive mode F, in other words, in a short time interval but long enough to determine the final state of the saddle crossings, the $\overline{q_F}$ can be identified as a ''good'' reaction coordinate. It is because there is no means or force returning the system to the new dividing surface $S(\overline{q_F}=0)$ even though the system may recross the original naive surface $S(q_F=0)$. The reformulated microcanonical (classical) TST rate constant $\overline{k}^{\text{TST}}$ is obtained[15] as a thermal average of the one-way fluxes j_+ $(=\dot{\overline{q}}_F(\mathbf{p},\mathbf{q})h(\dot{\overline{q}}_F(\mathbf{p},\mathbf{q})))$ across $S(\overline{q_F}=0)$ over microcanonical ensembles constructed over a range of energies E,

$$\begin{aligned}\overline{k}^{\text{TST}}(E)&=\langle j_+\rangle_E\\&=\langle \dot{\overline{q}}_F(\mathbf{p},\mathbf{q})\,\delta[\overline{q_F}(\mathbf{p},\mathbf{q})]h[\dot{\overline{q}}_F(\mathbf{p},\mathbf{q})]\rangle_E,\\&=\int_1 dq_1\,dp_1\cdots\int_N dq_N\,dp_N\delta[E-H(\mathbf{p},\mathbf{q})]\\&\quad\times\dot{\overline{q}}_F(\mathbf{p},\mathbf{q})\,\delta[\overline{q_F}(\mathbf{p},\mathbf{q})]h[\dot{\overline{q}}_F(\mathbf{p},\mathbf{q})],\end{aligned} \tag{31}$$

where $h(x)$ and $\delta(x)$, respectively, denote the Heaviside function and Dirac's delta function of x. The canonical form is also formulated straightforwardly.

If no approximate invariant of motion exists in the saddle region, $\overline{k}^{\text{TST}}(E)$ deviates from the (classically) exact reaction rate constant $k(E)$. Therefore one can introduce a new transmission coefficient κ_c, the deviation of the $\overline{k}^{\text{TST}}(E)$ from the $k(E)$:

$$k=\kappa_c\overline{k}^{\text{TST}}. \tag{32}$$

We may use κ_c to estimate the barrier recrossing effect, as a measure of the extent to which the quasi-invariants of motion associated with the reactive mode, i.e., the local action and its local frequency, cease to be approximate invariants. Their nonconstancy reflects the degree of *fully developed* chaos in which no invariant of motion exists, if the vibrational energy relaxation is fast enough to let us assume quasiequilibration in the well.

In order to focus on how the recrossings over a given dividing surface contribute to κ_c, we estimate the time-dependent quantities $\kappa_c^{\text{MD}}(t;S(\overline{q_F}^{i\text{th}}=0))$ in terms of our MD trajectories defined by

$$\kappa_c^{\text{MD}}(t;S(\overline{q_F}^{i\text{th}}=0))=\frac{\langle j(t=0)h[\overline{q_F}^{i\text{th}}(\mathbf{p},\mathbf{q})]\rangle_E}{\langle j_+(t=0)\rangle_E}, \tag{33}$$

where $j(t=0)$ and $j_+(t=0)$, respectively, denote the initial total and initial positive fluxes crossing the ith order LCPT dividing surface $S(\overline{q_F}^{i\text{th}}(\mathbf{p},\mathbf{q})=0)$. The origin of time t is taken to be zero when the system trajectory first crosses the given dividing surface. Equation (33) should also tell us how the vanishing of the approximate invariants of motion of the reactive mode reflects on the κ_c.

III. CALCULATIONS

In the present study we apply this method to saddle crossing dynamics in Ar_6, represented by the sum of pairwise Lennard-Jones potentials

$$V(\mathbf{r})=4\epsilon\sum_{i>j}^{N,N}\left[\left(\frac{\sigma}{r_{ij}}\right)^{12}-\left(\frac{\sigma}{r_{ij}}\right)^{6}\right]. \tag{34}$$

Here, if we assign laboratory scales of energy and length, we use values appropriate for argon, i.e., $\epsilon=121$ K and $\sigma=3.4$ Å with the atomic mass $m=39.948$ amu; the total linear and angular momenta are set to zero. This is the smallest inert gas cluster in which no saddle dynamics more regular than the dynamics within the local wells was revealed by the local K entropy analysis.[3] The potential energy profile is schematically shown in Fig. 1. This cluster has two kinds of potential energy minima. The global minimum corresponds to an octahedral arrangement of the atoms (OCT), with energy $E=-12.712\epsilon$, and the other higher minimum to the arrangement in which five atoms form a trigonal bipyramid, capped on one face by the sixth atom (CTBP), with energy $E=-12.303\epsilon$. There are two distinct kinds of first-rank saddles. One saddle at energy $E=-12.079\epsilon$ joins the OCT and the CTBP minima, whose fundamental (imaginary) frequency along the reaction coordinate q_F, $\omega_F=-49.29i$ cm^{-1}. The other higher saddle at energy $E=-11.630\epsilon$ joins two permutationally distinct CTBP structures, slightly flatter than the lower saddle, $\omega_F=-35.04i$ cm^{-1}. The fundamental frequencies at both saddles are listed in Table I. In the

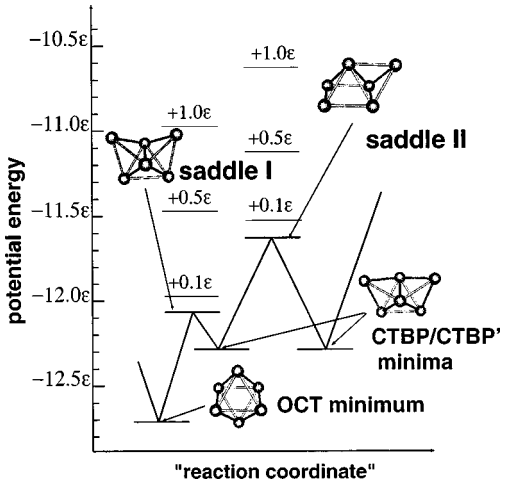

FIG. 1. A schematical picture of the potential energy surface of Ar_6. CTBP′ is a permutational isomer of the CTBP minimum neighboring on the OCT minimum.

present study we analyze the regularity at total energies in a range $E=0.1-1.0\epsilon$ above each saddle point energy, $E=-12.079\epsilon$ and $E=-11.630\epsilon$. Because the total angular momentum is zero, the chaotic behavior arises purely from the vibrational motion. (However vibrational modes may carry angular momentum, so that even in a state whose total angular momentum is zero, the internal and ''rigid body'' angular momenta may be nonzero.) The $3N$-6(=12)-DOF regional Hamiltonian is constructed from the zeroth-order harmonic oscillator Hamiltonian including one parabolic barrier coordinate q_F, and the three-, and four-body nonlinear couplings expressed in arbitrary combinations of the normal coordinates $\mathbf{q}$. It is obtained by calculating the second-(=Hessian), third-, and fourth-order energy derivatives with respect to $\mathbf{r}$ at the saddle, and then applying a projection operator[26] to eliminate the translational and (infinitesimal) rotational motions. For the sake of simplicity we introduced a cutoff value δ_V for estimating the three-, and four-body nonlinear couplings terms such that all the terms whose coefficients are smaller than δ_V in magnitude are neglected. Setting δ_V to be 2×10^{-5}, we found the total numbers of the three-, and four-body terms to be 106 and 365 for saddle I, and 189 and 674 for saddle II, respectively.[34] Throughout this paper the parabolic barrier coordinate F in the original $(\mathbf{p},\mathbf{q})$ space [and in the new $(\bar{\mathbf{p}},\bar{\mathbf{q}})$ space] is denoted as q_1 ($\bar{q}_1$) and the other bath coordinates as $q_2,q_3,\ldots,q_{12}$ ($\bar{q}_2,\bar{q}_3,\ldots,\bar{q}_{12}$) in such an order that $\omega_2 \leqslant \omega_3,\ldots,\leqslant\omega_{12}$ ($\bar{\omega}_2\leqslant\bar{\omega}_3,\ldots,\leqslant\bar{\omega}_{12}$), and the units of energy, coordinate, momentum, action, frequency, and time are ϵ, $m^{1/2}\sigma$, $m^{1/2}\sigma\,\mathrm{ps}^{-1}$, Kps, ps^{-1}, and ps, unless otherwise noted.

TABLE I. The fundamental frequencies ω_k for saddles I and II (cm^{-1}).

Mode	Saddle I	Saddle II
1	$-49.29i$(-1.477i)[a]	$-35.04i$(-1.050i)
2	96.06(2.880)	89.01 (2.668)
3	113.04(3.389)	98.54 (2.954)
4	122.91(3.684)	124.37(3.729)
5	149.40(4.478)	138.24(4.144)
6	149.71(4.488)	153.00(4.587)
7	173.06(5.188)	171.13(5.130)
8	197.81(5.930)	178.34(5.346)
9	200.03(5.996)	198.44(5.949)
10	206.19(6.181)	206.63(6.195)
11	235.10(7.047)	229.78(6.889)
12	238.47(7.148)	241.04(7.226)

[a]The values in the parentheses are ω_k in units of ps^{-1}.

The trajectories from a minimum rarely cross the energy barrier at an energy much higher than E/f where E and f are the total energy of the system and the number of DOF, respectively. Many very long and accurate trajectories would be required for robust analyses of infrequent saddle crossings, if they were to be extracted directly from trajectories. Hence for analyses of the infrequent saddle crossings, we employed an efficient sampling method.

(i) We generated the microcanonical ensemble on the dividing surface $S(q_1=0)$:[35–39] First, we prepared ten initial conditions by using a random number generator to systematically position the system under constraint of $p_1=0$ and $q_1=0$ in the phase space. The total energy was set to a desired value by scaling the momenta uniformly. For the ten independent seeds, we performed constant-energy MD calculations under the constraint of $p_1=0$ and $q_1=0$. After the system is equilibrated by a 3000-step MD trajectory calculation initiated from each independent seed, we recorded the coordinate files consecutively at every 300-step interval until 1000 coordinate files have accumulated. Then, to generate the total set of configurations, we sampled all the momenta including p_1 microcanonically.

(ii) Depending on the location on the q_1 axis of $S(\bar{q}_1^{i\mathrm{th}}(\mathbf{p},\mathbf{q})=0)(i>0)$, the system trajectories initiated from $S(q_1=0)$ do not necessarily cross the $S(\bar{q}_1^{i\mathrm{th}}(\mathbf{p},\mathbf{q})=0)$ even though all of them cross the naive $S(q_1=0)$ at $t=0$. Therefore, in order to sample the crossing trajectories over $S(\bar{q}_1(\mathbf{p},\mathbf{q})=0)$ more efficiently, we calculated the time-reversed trajectory from $S(q_1=0)$ by replacing $\mathbf{p}(t=0)=-\mathbf{p}(t=0)$ for each initiated trajectory on $S(q_1=0)$, and generated one ''well–saddle–well'' crossing trajectory made from these two trajectories as one sampled trajectory.

For the trajectory calculations we used a fourth-order Runge–Kutta method[40] with adaptive step-size control, which dynamically adjusts the step size to reduce the error of integration in calculation. The total energies in our MD calculations were conserved within $\pm1\times10^{-6}\epsilon$. It was found that the 10 000 trajectories are enough to yield statistical convergence in calculating the $\kappa_c^{\mathrm{MD}}(t;S(\bar{q}_1^{i\mathrm{th}}(\mathbf{p},\mathbf{q})=0))$ for $i=0,1,2$ at three total energies, 0.1, 0.5, and 1.0 ϵ.

IV. RESULTS AND DISCUSSIONS

We first investigate the dynamics of crossing over saddle I, linking the global minimum OCT and the higher minimum CTBP. Figure 2 shows a representative trajectory projected onto the (q_1,q_{12}) plane for each total energy, 0.05, and 0.5ϵ above the saddle point energy. Here the trajectory at 0.05ϵ is shown specifically because intuition tells us it should be less chaotic than those at $0.1-1.0\epsilon$. This is because at such an

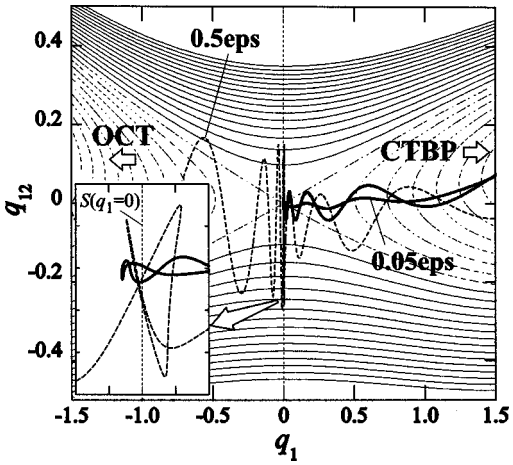

FIG. 2. A representative saddle-recrossing trajectory at each energy, 0.05 and 0.5ϵ over the dividing surface $S(q_1=0)$, projected onto the (q_1,q_{12}) plane and PES contour plot in this plane. The window is scaled to $-0.01<q_1<0.01$ and $-0.3<q_{12}<0.2$. The trajectories from the left- to the right-hand side correspond to crossing from the OCT to the CTBP minimum. While the sampled trajectory at 0.05ϵ (the bold solid line) is nonreactive, i.e., coming from the CTBP and returning to the same CTBP, that at $E=0.5\epsilon$ (the dashed line) is reactive. The PES contour is plotted with an energy step 0.03ϵ, whose solid and dashed lines represent positive and negative values, respectively.

energy, in the vicinity of the transition state, the system has insufficient kinetic energy to reach regions where nonlinearity, anharmonicity, and mode–mode mixing are significant.

To begin, we may look into the new action variables $\overline{J}_k(\mathbf{p},\mathbf{q})$ along the saddle-crossing trajectories obeying equations of motion of the original Hamiltonian $H(\mathbf{p},\mathbf{q})$. The trajectory of an isolated bound oscillator retraces the same points during each oscillation and the associated action is a constant of the motion. The extent to which the new kth action $\overline{J}_k(\mathbf{p},\mathbf{q})$ mimics this behavior indicates how separable the new kth mode, described by $\overline{p}_k$ and $\overline{q}_k$, is. Figure 3 shows the zeroth-, first-, and second-order new actions along the trajectory at 0.05ϵ. At even $E=0.05\epsilon$, only slightly above the saddle point energy, almost all the zeroth-order actions $\overline{\mathbf{J}}^{0\text{th}}(\mathbf{p},\mathbf{q})$ do not maintain constancy of motion at all. This result implies that the system's trajectory reflects even very small nonlinearities on the PES and deviates from a simple normal mode picture. As we extend the order of LCPT, some but not all LCPT actions $\overline{J}_k$ tend to be conserved in the saddle region. Figure 4 shows the zeroth-, first-, and second-order $\overline{J}_k(t)$ for $k=1,3,4$, and 8 on the same figure axes. Figure 4 shows that the higher the order to which the LCPT is carried, the more *some* of the actions $\overline{J}_k$ tend to be well-conserved, and to persist as nearly conserved quantities for longer time periods. Second-order LCPT can extract ''good'' invariants of motion associated with the modes $\overline{q}_1^{2\text{nd}}$, $\overline{q}_3^{2\text{nd}}$, and $\overline{q}_8^{2\text{nd}}$ in the saddle region. (The transformed actions $\overline{J}_k^{2\text{nd}}$ are well conserved within ± 0.01 Kps.) On the other hand for mode 4, although LCPT seemingly improves the constancy of $\overline{J}_4(\mathbf{p},\mathbf{q})$ in the zeroth-order estimate, the second-order LCPT does not yield a good invariant of motion for this mode, compared with modes 1, 3, and 8. The

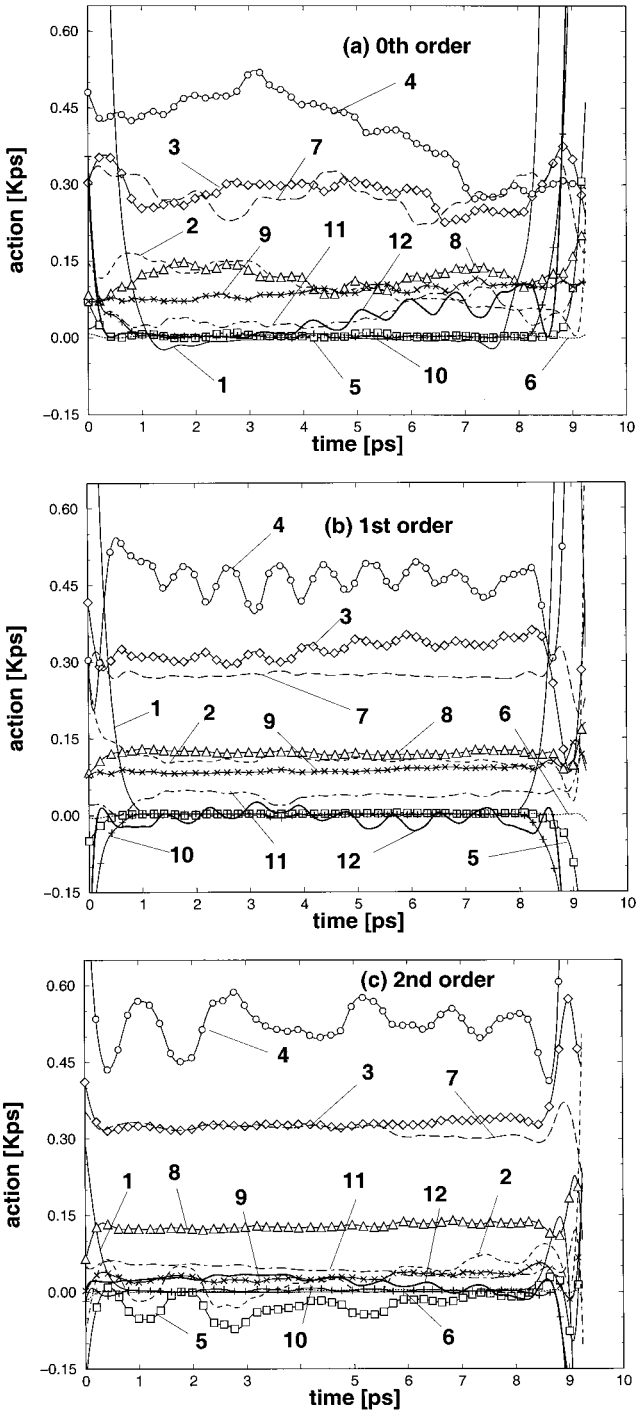

FIG. 3. The time dependencies of $\overline{J}_k(\mathbf{p},\mathbf{q})$ for the saddle-crossing trajectory at 0.05ϵ in Fig. 2: (a) zeroth; (b) first; and (c) second-order actions. The units of action for mode 1 must be multiplied by a factor of an imaginary number i because it is imaginary throughout the following figures. In $1.5<t<7.5$ ps, the system trajectories remain in a region $\sim -0.01<q_1<0.2$ $[m^{1/2}\sigma]$. The solid, dashed, diamond, circle, square, dotted, long-dashed, triangle, x, +, dot-dashed, and bold-solid lines denote throughout this paper 1, 2, 3, 4, 5, 6, 7, 8, 9, 10, 11, and 12, respectively, unless noted otherwise.

initial drop observed in the $\overline{J}_1^{2\text{nd}}$ at short times (e.g., 0–0.5 ps in Fig. 4) to the flat region implies that initially, the system is just entering a ''regular region'' near the saddle point, outside of which the system is subject to considerable nonlin-

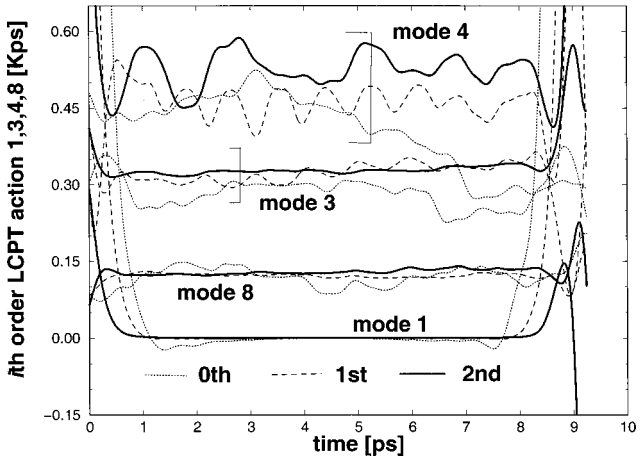

FIG. 4. The action $\overline{J}_k(\mathbf{p},\mathbf{q})$ ($k=1,3,4,8$) at 0.05ϵ in Fig. 2. The dash-dot, dash, and bold-solid lines denote the zeroth-, first-, and second-order actions, respectively.

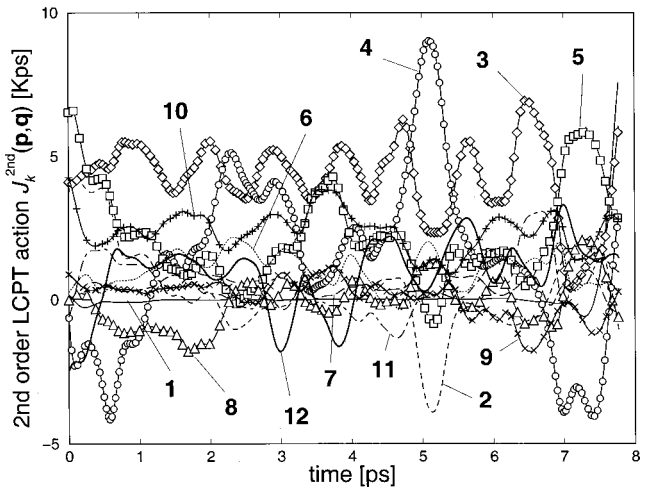

FIG. 5. The time dependencies of the second order action $\overline{J}_k(\mathbf{p},\mathbf{q})$ for the saddle-crossing trajectory at $E=0.5\epsilon$ in Fig. 2. In $1.5<t<6$ ps, the system trajectories remain in a region $\sim -0.2<q_1<0.2$ $[m^{1/2}\sigma]$. The meanings of each line are given in the caption of Fig. 3.

earities of the PES; in that region away from the saddle, we can expect to find no approximate invariant of motion at any given finite order of LCPT.[1–3]

At this energy, all the associated second-order frequencies $\overline{\omega}_k^{2\mathrm{nd}}(\mathbf{p},\mathbf{q})(1\leqslant k\leqslant 12)$ remain approximately constant within $\pm 0.01\,\mathrm{ps}^{-1}$ through the saddle region. In contrast to the normal modes' frequencies at saddle points, the LCPT frequencies $\overline{\omega}_k(\mathbf{p},\mathbf{q})$ could depend, in principal, on the incident coordinates and momenta $(\mathbf{p}(0),\mathbf{q}(0))$ going into the saddle region, although the $\overline{\omega}_k(\mathbf{p},\mathbf{q})$ should be conserved on a trajectory when it has entered the saddle region if the regional crossing motion can be considered as ''quasiregular'' at the order of the perturbative calculation performed.

This implies (at least for the sampled trajectory) that some modes are well decoupled and follow periodic orbits in phase space such as those of Eqs. (12) and (13), while the others are coupled at least within coupled-mode subsets in the $(\overline{\mathbf{p}}^{2\mathrm{nd}},\overline{\mathbf{q}}^{2\mathrm{nd}})$ coordinate system. At such an energy, slightly above the saddle point, where the nonlinearity of the PES [Eq. (17)] may be regarded as a ''sufficiently weak perturbation,'' this nonconstancy of some actions must be indicating that still higher-order LCPT is required to extract M *local* invariants of motion in the saddle region from the M-DOF Hamiltonian system (i.e., KAM torus[18]), even though the second-order LCPT is adequate to reveal some invariants of motion. It is also not apparent how far a region of regularity would extend in higher orders.

How does the crossing dynamics change as the energy of the system increases? Intuition suggests that at higher total energies, the nonlinearities of the PES cannot be considered as a ''sufficiently weak perturbation,'' and the number of approximate local invariants of motion in the phase space becomes smaller and smaller, going to zero at sufficiently high energy. Consequently the local crossing dynamics should change from quasiregular to chaotic, with increasing energy. In fact, Fig. 5 shows the second-order $\overline{J}_k(t)$ along a sample trajectory at $E=0.5\epsilon$, ten times higher than 0.05ϵ where the crossing behavior is quite regular. At this higher energy, almost none of the action variables are conserved locally, even through second order of LCPT. However the one variable that stands out among all the rest is the reaction coordinate, whose action is nearly conserved, while *no approximate invariant of motion can be found for the bath modes,* $\overline{q}_k$ $(k=2,3,\ldots,M)$, *only the action variable of the reactive mode* $\overline{q}_1$ *becomes more regular and well-conserved as the LCPT order increases* (see Fig. 6). Figure 7 shows the second-order LCPT frequencies $\overline{\omega}_k^{2\mathrm{nd}}(\mathbf{p},\mathbf{q})$ along the same trajectory. Compared with the case at $E=0.05\epsilon$, almost all frequencies $\overline{\omega}_k^{2\mathrm{nd}}(\mathbf{p},\mathbf{q})$ deviate significantly from the fundamental frequencies ω_k. However the reactive coordinate's frequency $\overline{\omega}_1^{2\mathrm{nd}}(\mathbf{p},\mathbf{q})$ is well conserved during the saddle crossing, as well as the action $\overline{J}_1$ is.

This result implies that, while the DOF of the bath, i.e., all the other modes, establish their own $(M-1)$-dimensional subspace Z, and the projections of any crossing dynamics onto the subspace Z must be regarded as chaotic, the new

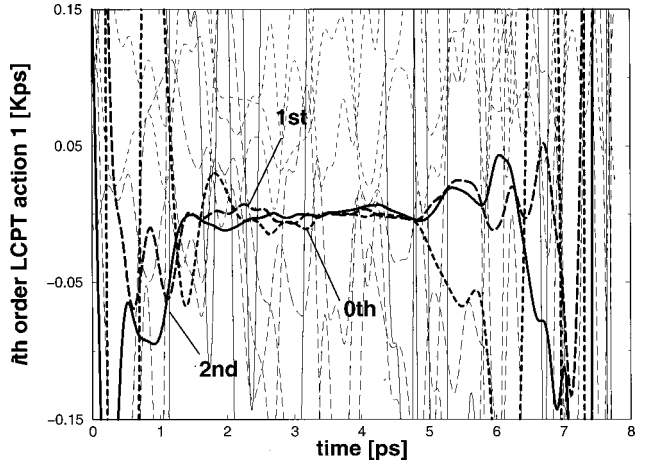

FIG. 6. The action $\overline{J}_1(\mathbf{p},\mathbf{q})$ at 0.5ϵ in Fig. 2. The dash-dot, dash, and solid lines denote the zeroth-, first-, and second-order actions. The actions of mode 1 are emphasized by the bold lines.

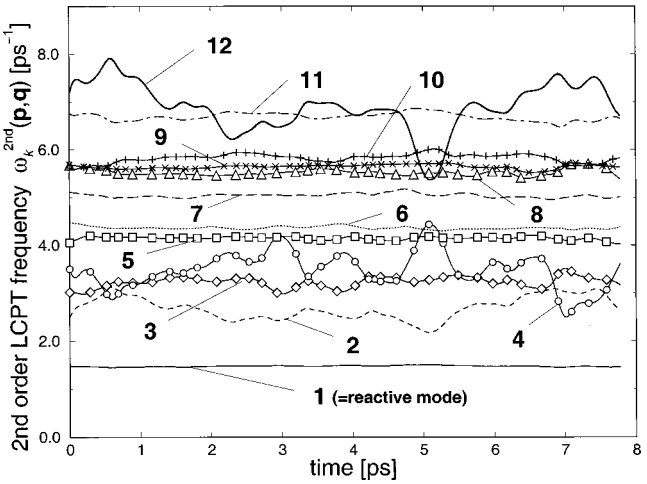

FIG. 7. The second order frequencies $\bar{\omega}_k^{2nd}(\mathbf{p},\mathbf{q})$ at 0.5ϵ in Fig. 2. Again, the unit of frequency for mode 1 must be multiplied by a factor of $-i$.

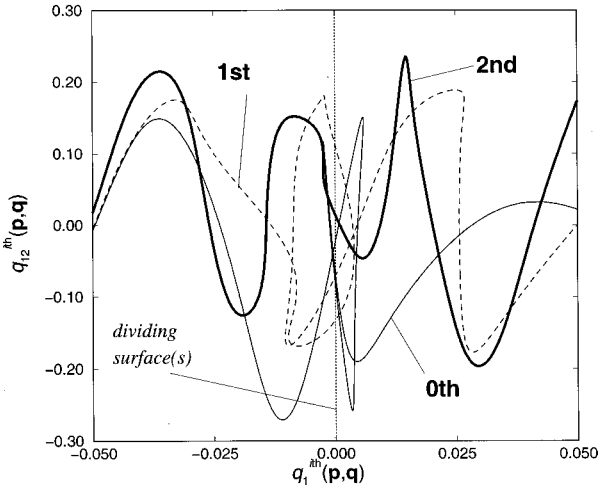

FIG. 9. The projections of the recrossing trajectory at 0.5ϵ in Fig. 2 onto the zeroth-, first-, and second-order $(\bar{q}_1(\mathbf{p},\mathbf{q}),\bar{q}_{12}(\mathbf{p},\mathbf{q}))$ plane.

reactive mode is well decoupled from the Z space, and is governed by a hyperbolic orbit in phase space represented by Eqs. (12) and (13) during saddle crossings.

Next, how do these saddle crossing trajectories actually look in the $(\bar{\mathbf{p}},\bar{\mathbf{q}})$ space? The projections of the ''recrossing'' trajectories at $E=0.05$ and 0.5ϵ onto the zeroth-, first-, and second-order new coordinate planes of $\bar{q}_1(\mathbf{p},\mathbf{q})$ and $\bar{q}_{12}(\mathbf{p},\mathbf{q})$ are shown in Figs. 8 and 9. Here the zeroth-order coordinate system $(\bar{\mathbf{p}}^{0th},\bar{\mathbf{q}}^{0th})$ is the original $(\mathbf{p},\mathbf{q})$ system we have used to describe the cluster. The abscissas in Figs. 8 and 9 correspond to a reaction coordinate, i.e., $\bar{\omega}_1 \in \Im$, and the ordinates, to the fastest bath coordinates, i.e., $\bar{\omega}_{12} \in \Re$, in each order coordinate system.

To do this, we first examine the nonreactive *re*crossing trajectory at 0.05ϵ (see Fig. 8), the nonreactive recrossing motion over the naive dividing surface $S(q_1=0)$. In first and second order, this trajectory never crosses any dividing surface $S(\bar{q}_1^{1st}(\mathbf{p},\mathbf{q})=0)$ and $S(\bar{q}_1^{2nd}(\mathbf{p},\mathbf{q})=0)$ from the CTBP minimum where the trajectory originates. We can deduce one important feature from Fig. 8: if local invariants of motion associated with the higher-order reactive LCPT coordinate, e.g., $\bar{q}_1^{2nd}$, exist, any nonreactive recrossing trajectories observed over the naive dividing surface $S(q_1=0)$ transform to trajectories that do not cross the LCPT dividing surface, $S(\bar{q}_1^{2nd}(\mathbf{p},\mathbf{q})=0)$, in higher orders of LCPT. This is because decoupling the motion along the reactive LCPT coordinate removes all forces that would return the system back across the dividing surface. Such nonreactive trajectories are those with insufficient incident momentum in the reactive coordinate $\bar{p}_1(\mathbf{p}(0),\mathbf{q}(0))$ to climb over the saddle.

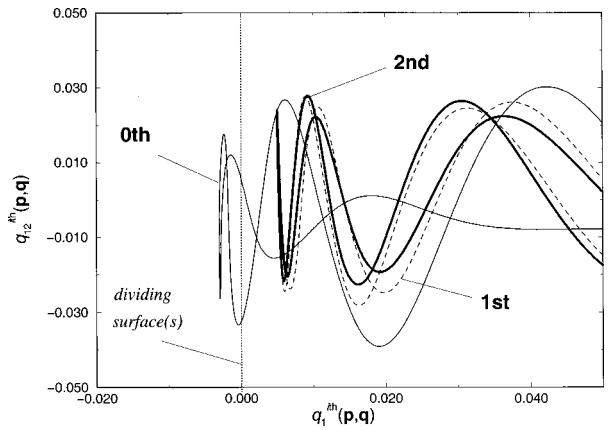

FIG. 8. The projections of the recrossing trajectory at 0.05ϵ in Fig. 2 onto the zeroth-, first-, and second-order $(\bar{q}_1(\mathbf{p},\mathbf{q}),\bar{q}_{12}(\mathbf{p},\mathbf{q}))$ plane.

A consequence of the LCPT transformation that is perhaps even more striking appears in the behavior of the reactive *re*crossing trajectory at 0.5ϵ in Fig. 9. Here, the recrossings that occur over the naive dividing surface $S(q_1=0)$ in zeroth order are eliminated; they occur as no-return crossing motions over the second-order dividing surface $S(\bar{q}_1^{2nd}(\mathbf{p},\mathbf{q})=0)$. Furthermore the system's trajectories along the second-order reactive coordinate $\bar{q}_1^{2nd}$ are not forced to return to the dividing surface $S(\bar{q}_1^{2nd}=0)$ over the (saddle) region, $-0.05<\bar{q}_1^{2nd}<0.05$. On the other hand, the zeroth- and first-order LCPT coordinates are not decoupled from the other modes in the regions either near or more distant from the dividing surface. This shows that no approximate invariant of action exists in zeroth- or first-order $\bar{q}_1$ in the saddle region (see Fig. 6). (Recall that any zeroth-order LCPT coordinate can be decoupled in the infinitesimally small region around a stationary point). However the second-order LCPT coordinate systems are effectively decoupled to rotate away the apparent recrossings of the zeroth-order $S(q_1=0)$ to the single crossing motion over the LCPT dividing surface $S(\bar{q}_1^{2nd}=0)$.

Thus far, we have used representative trajectories crossing saddle I at $E=0.05$ and 0.5ϵ to show how topological change in saddle-crossing dynamics emerges as the total energy of the system increases. Many saddle-crossing trajectories randomly sampled at $E=0.1-1.0\epsilon$ above the saddle points I and II appear to maintain at least one approximate constant of action, that of the reactive degree of freedom. To verify this, we scrutinize the separability of the reactive co-

TABLE II. The classifications of 10,000 saddle crossing trajectories across the ith order phase space dividing surface $S(\overline{q_1^{i\text{th}}}(\mathbf{p},\mathbf{q})=0)$ for each saddle I and saddle II at $E=0.1-1.0\epsilon$ above each saddle point energy E_{sp}.

	Saddle I ($E_{sp}=-12.079\epsilon$)									Saddle II ($E_{sp}=-11.630\epsilon$)								
$E=$	0.1ϵ			0.5ϵ			1.0ϵ			0.1ϵ			0.5ϵ			1.0ϵ		
No. of crossings	0th[a]	1st	2nd	0th	1st	2nd	0th	1st	2nd	0th	1st	2nd	0th	1st	2nd	0th	1st	2nd
1	9783	9793	9805	9523	9492	9555	9426	9329	9395	9803	9859	9870	9589	9616	9661	9493	9425	9419
2	187	4		396	47	5	455	81	26	104	6	2	258	40	8	325	77	45
3	22	10		47	66	12	74	141	95	62	11	1	106	100	38	110	166	166
4	8	2		29	5	4	34	16	9	22	4		28	14	9	44	26	25
5		1		3	13	3	8	29	12	6	2		17	11	11	20	25	29
6		0		1	2	1	3	2	6	2	1		0	5	3	6	13	15
7		1		0	2	3		4	3	1			1	6	2	2	6	9
8				1	0			1	3				1	4	1		0	5
9					0			2	1								3	0
10					1			0	0								2	2
11								1	1									1
12								1										

[a]0th, 1st, and 2nd indicate the order of the phase space dividing surface. The zeroth order corresponds to the conventional dividing surface $S(q_1=0)$ using a reactive normal coordinate.

ordinate $\overline{q_1}$ from the Z subspace of the bath DOF for saddles I and II by classifying the 10 000 saddle crossing trajectories generated in Sec. III according to the number of times each crosses the dividing surface $S(\overline{q_1}=0)$ in either direction. Table II shows the classifications of the saddle crossing trajectories at each $E=0.1$, 0.5, and 1.0ϵ above each saddle point energy of saddles I and II, respectively.

At the small total energies of $E=0.1\epsilon$ for both the saddles, the numbers of recrossing trajectories observed over $S(q_1=0)$ are drastically reduced in the LCPT coordinate systems. The higher the order of the LCPT, the greater the number of recrossings rotated away to the no-return crossing trajectories over the phase space dividing surface $S(\overline{q_1^{i\text{th}}}(\mathbf{p},\mathbf{q})=0)(i>0)$. Thus, the number of recrossing trajectories over the given dividing surfaces decreases, 217(0) $\rightarrow$18(1)$\rightarrow$0(2) at saddle I and 197(0)$\rightarrow$24(1)$\rightarrow$3(2) at saddle II, with the increase of the order of LCPT indicated in the parentheses. Note that the recrossings over $S(q_1=0)$ at saddle I are *all* eliminated at the second order. The three recrossing trajectories observed over $S(\overline{q_1^{2\text{nd}}}(\mathbf{p},\mathbf{q})=0)$ for saddle II imply that the second order is not sufficient to completely decouple the reactive coordinate $\overline{q_1}$ from the other bath coordinates, in contrast to the saddle I crossings.

At the higher total energies the numbers of recrossing trajectories over the configurational dividing surface $S(q_1=0)$ increase, 217(at $E=0.1\epsilon$)$\rightarrow$477(0.5ϵ)$\rightarrow$574(1.0ϵ) at saddle I and 197(at $E=0.1\epsilon$)$\rightarrow$411(0.5ϵ)$\rightarrow$507(1.0ϵ) at saddle II. Furthermore, the recrossing trajectories tend to cross $S(q_1=0)$ more frequently before reaching the final state, i.e., the population of the recrossing trajectories whose number of crossings is relatively large increases. This is because, as the total energy increases, the system's trajectories find higher nonlinearities of the PES, and the bottleneck separating the two stable states extends to a larger space from the saddle point.[41] In consequence, although the second-order LCPT surface has fewer recrossing trajectories than the zeroth-order surface at $E=0.5\epsilon$ and 1.0ϵ, the second-order LCPT does not completely decouple the reactive coordinate $\overline{q_1}$ from the Z subspace of the bath DOF and leaves more recrossing trajectories at the higher total energy, i.e., $0(0.1\epsilon)\rightarrow28(0.5\epsilon)\rightarrow156(1.0\epsilon)$ at saddle I and $3(0.1\epsilon)\rightarrow72(0.5\epsilon)\rightarrow297(1.0\epsilon)$ at saddle II.

Up to about 0.1ϵ, traces of separability remain in several degrees of freedom in the second-order $(\overline{\mathbf{p},\mathbf{q}})$ space, and the reactive degree of freedom is clearly decoupled from the others. In the higher energy regime $\geqslant1.0\epsilon$, even the reactive mode becomes coupled with all the other degrees of freedom, the trajectories become fully chaotic and show recrossings, losing all the simplicity apparent at lower energies.

Let us now examine the new transmission coefficient $\kappa_c^{\text{MD}}(t;S(\overline{q_1^{i\text{th}}}=0))(i=1,2)$, to see how it behaves in terms of the new dividing surface. Figures 10 and 11 show

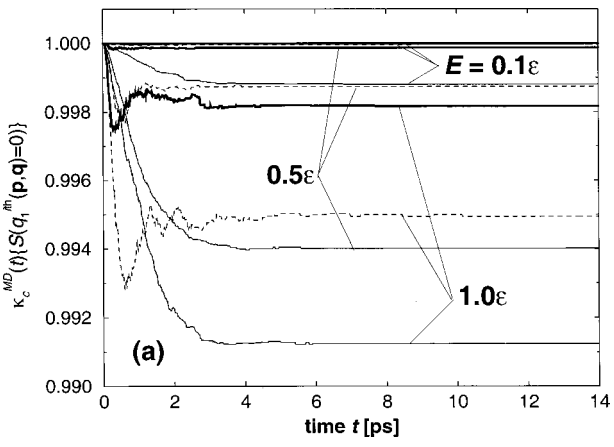

FIG. 10. The transmission coefficient $\kappa_c^{\text{MD}}(t;S(\overline{q_1^{i\text{th}}}(\mathbf{p},\mathbf{q})=0))(i=0,1,2)$ at $E=0.1$, 0.5, and 1.0ϵ for saddle I. The solid, dashed, and bold-solid lines denote $\kappa_c^{\text{MD}}(t;S(\overline{q_1^{i\text{th}}}(\mathbf{p},\mathbf{q})=0))$ in terms of the zeroth-, first-, and second-order dividing surface, respectively. The convergent values are 0.9988(0), 0.99996(1), 1.00000(2) (at $E=0.1\epsilon$); 0.9940(0), 0.9987(1), 0.9999(2) (at $E=0.5\epsilon$); 0.9912(0), 0.9949(1), 0.9982(2) (at $E=1.0\epsilon$) where the number in parentheses is the order of the LCPT.

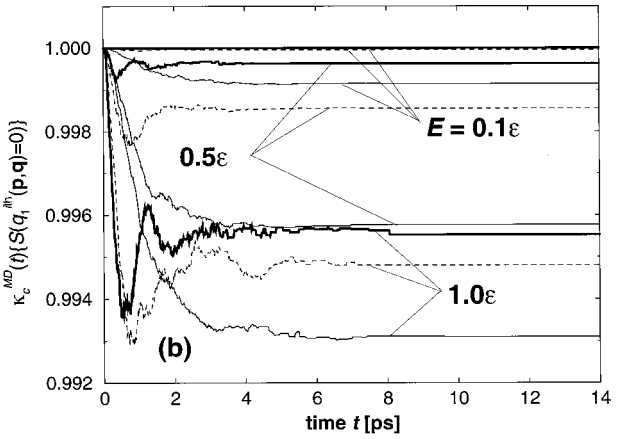

FIG. 11. The transmission coefficient $\kappa_c^{\mathrm{MD}}(t;S(\overline{q_1^{i\mathrm{th}}}(\mathbf{p},\mathbf{q})=0))(i=0,1,2)$ at $E=0.1$, 0.5, and 1.0ϵ for saddle II. The meaning of each line is given in the caption of Fig. 10. The convergent values are 0.9991(0), 0.99995(1), 1.00000(2) (at $E=0.1\epsilon$); 0.9958(0), 0.9986(1), 0.9996(2) (at $E=0.5\epsilon$); 0.9931(0), 0.9948(1), 0.9955(2) (at $E=1.0\epsilon$) where the number in parentheses is the order of the LCPT.

$\kappa_c^{\mathrm{MD}}(t;S(\overline{q_1^{i\mathrm{th}}}(\mathbf{p},\mathbf{q})=0))(i=0,1,2)$ at three different energies above each saddle point energy for saddles I and II, respectively. The zeroth-order estimation $\kappa_c^{\mathrm{MD}}(t;S(\overline{q_1^{0\mathrm{th}}}=0))$ corresponds to the conventional MD transmission coefficient $\kappa^{\mathrm{MD}}(t)$ based on $S(q_1=0)$.

As the data in Table II show, the zero-order $\kappa^{\mathrm{MD}}(t)$ deviates significantly from unity (except at a very short times) and these deviations increase with increasing total energy. The plateau in $\kappa^{\mathrm{MD}}(t)$ apparent in Figs. 10 and 11 implies that the recrossing trajectories eventually go into their final state and never again cross the given dividing surface after a certain time.[42] The plateau value could be referred to as the conventional transmission coefficient κ. All these κ's from $E=0.1$ to 1.0ϵ above the saddle point energy are smaller for saddle I than for saddle II, namely: $0.9988(\mathrm{I})<0.9991(\mathrm{II})$ (at $E=0.1\epsilon)\rightarrow 0.9940(\mathrm{I})<0.9958(\mathrm{II})$ $(0.5\epsilon)\rightarrow 0.9912(\mathrm{I})<0.9931(\mathrm{II})$ (1.0ϵ) (The number in the parentheses denotes either saddle I or II). These results show that the traditional reaction coordinate q_1 for saddle I is more coupled to the other bath DOF $q_k(k\neq 1)$ than for saddle II. This is consistent with the previous observations for small inert gas clusters[3,43,44] that sharper saddles tend to yield more chaotic cluster dynamics close to the saddle point; those conclusions were based on the high positive correlation of the local K entropy in the saddle region with the degree of the negative curvature along the hyperbolic normal coordinate at the saddle point.

Turning to the transmission coefficient in the transformed coordinates, we now show for both saddles that for low and moderately high energies, the higher the order of the perturbative calculation, the closer the $\kappa_c^{\mathrm{MD}}(t;S(\overline{q_1^{i\mathrm{th}}}=0))$ is to unity. In fact for low total energy, $E=0.1\epsilon$, the converged values of $\kappa_c^{\mathrm{MD}}(t;S(\overline{q_1^{2\mathrm{nd}}}=0))$, which we designate $\kappa_c(S(\overline{q_1^{2\mathrm{nd}}}=0))$, are 1.000 00 for both saddles, to six significant figures. [The precision of the molecular dynamics calculation is approximately this for individual trajectories of about 5– 10 000 time steps, well beyond the 3–5000 steps we used to find κ_c. Our values are based on averaging 10^4 trajectories. It is the nominal variance of these averages that is less than 10^{-6}. Hence the value of $\kappa_c(S(\overline{q_1^{2\mathrm{nd}}}=0))$ is indistinguishable from unity within the limits of the computation.] Even at energies $\sim 0.5\epsilon$, where the saddle crossing dynamics is chaotic, that is, where almost all actions exhibit no evidence of being approximate invariants of motion, the converged values of $\kappa_c(S(\overline{q_1^{2\mathrm{nd}}}=0))$ are almost unity, e.g., 0.9999 (for saddle I) and 0.9996 (for saddle II) at $E=0.5\epsilon$. As the total energy becomes much higher, converged values of $\kappa_c(S(\overline{q_1^{2\mathrm{nd}}}=0))$ deviate significantly from unity. We interpret this deviation from unity as a measure of the insufficiency of second-order LCPT to decouple the reactive coordinate $\overline{q_1}$ from the Z subspace of the bath DOF, i.e., the difficulty of exposing the approximate invariants of motion associated with $\overline{q_1}$ with only a few orders of perturbation. (The possibility must also be considered that at sufficiently high energies, perturbation theory will not be convergent and a nonperturbative approach would be required to show the approximate local invariants in any but a very small region.) Accordingly, the crossing dynamics over saddle I should exhibit better approximate invariants of motion with $\overline{q_1}$ than that over saddle II at the second order, because the deviation is smaller for saddle I than that for saddle II. Note that less chaotic saddle-crossing dynamics need not imply a better approximate invariant of motion associated with $\overline{q_1}$ at any specific order of the perturbative calculation. Furthermore, the strength of chaos, as characterized by the local Kolmogorov entropy, the sum of all the positive (local) Liapunov exponents $\boldsymbol{\lambda}^{\mathrm{sad}}$, is only weakly affected by a single small positive exponent λ_1^{sad} associated with the somewhat-regularized $\overline{q_1}(\mathbf{p},\mathbf{q})$ motion. This ''burial'' of a few locally regular modes in a sea of chaotic modes is apparent in the results of Hinde and Berry.[3] Our result implies that, even in the region where the system is almost chaotic, an approximate analytical expression for (first-rank) saddle-crossing dynamics may nonetheless exist along a negatively curved coordinate in the $(\overline{\mathbf{p}},\overline{\mathbf{q}})$ space.

V. SUMMARY AND CONCLUDING REMARKS

We found, with the analysis afforded by the minimal-recrossing trajectories provided by the LCPT analysis, that there are at least three distinct energy regions above the saddle point energy that can be classified in terms of the regularity of saddle-crossing dynamics. Let us now articulate the distinctions among them.

1. Quasiregular region. All or almost all the degrees of freedom of the system *locally* maintain approximate constants of motion in the region of the transition state. The saddle crossing dynamics from well to well is fully deterministic, obeying M-analytical solutions [see Eqs. (12) and (13)] for systems of M degrees of freedom. The dynamical correlation between incoming and outgoing trajectories from and to the transition state region is quite strong, and the dimensionality of saddle crossings is essentially one, corresponding to the reactive mode $\overline{q_F}$ in the $(\overline{\mathbf{p}},\overline{\mathbf{q}})$ space. Barrier recrossing motions observed over a naive dividing surface

defined in the configuration space are *all* rotated away to no-return single crossing motions across a phase space dividing surface $S(\overline{q_F}(\mathbf{p},\mathbf{q})=0)$. If the vibrational energy relaxes fast enough to let us assume quasiequilibration in the wells, the initial conditions $(\overline{\mathbf{p}}(0),\overline{\mathbf{q}}(0))$ of the system as it enters the transition state from either of the stable states can be simply sampled from microcanonical ensembles. One may then evaluate the (classical) exact rate constant, free from the recrossing problem. The staircase energy dependence observed by Lovejoy *et al.*[6] for highly vibrationally excited ketene indicates that the transverse vibrational modes might indeed be approximately invariants of motion.[7] We classify such a range of energy, in which the rate coefficient shows staircase structure, as corresponding to this quasiregular region.

2. Intermediate, semichaotic region Due both to significant (near) resonances and to strong anharmonic mode–mode couplings emerging at these intermediate energies, *almost* all the approximate invariants of motion disappear, consequently inducing a topological change in dynamics from quasiregular to chaotic saddle crossings. However at least one approximate invariant of motion survives during the saddle crossings, associated with the reactive coordinate $\overline{q_F}(\mathbf{p},\mathbf{q})$. This is due to the fact that an arbitrary combination of modes cannot satisfy the resonance conditions of Eq. (14) if one mode having an imaginary frequency, the reactive mode in this case, is included in the combination. The other frequencies associated with bath modes fall on the real axis, orthogonal to the imaginary axis in the complex $\boldsymbol{\omega}$ plane. That is,

$$\left|\sum_{k=1}^{M}{}^{\dagger} n_k\omega_k\right| \geqslant |\omega_F| > O(\epsilon^n) \tag{35}$$

for arbitrary integers n_k with $n_F \neq 0$, where $\Sigma^{\dagger}$ denotes the combination including the reactive mode. This was first pointed out by Miller *et al.* in their semiclassical TST studies.[31] In this region the dynamical correlation between incoming and outgoing trajectories to and from the transition state becomes weak (but nonzero!), and the saddle crossings' dimensionality is $\simeq M-1$, excluding the one dimension of $\overline{q_F}$, in this region. If the associated imaginary frequency $\overline{\omega_F}(\mathbf{p},\mathbf{q})$ is approximately constant during a saddle crossing as the action $\overline{J_F}(\mathbf{p},\mathbf{q})$ is,[45] the reaction coordinate $\overline{q_F}$ decouples from the Z subspace composed of the other bath DOF, in which the system dynamics is manifestly chaotic. The $\overline{q_F}$ dynamics is then represented analytically during saddle crossings, and a dividing surface $S(\overline{q_F}(\mathbf{p},\mathbf{q})=0)$ can still be extracted free from the barrier recrossings, even for saddle crossings chaotic in the bath modes.

We may expect that various kinds of resonance zones[18,46] occur in the transition state region, densely distributed, associated with very complicated patterns of level crossings in phase space, in a so-called ''Arnold web.''[18] The transport among the states in such a web in many-DOF systems raises many interesting and unresolved questions.[10,46,47] By using local frequency analysis, Martens, Davis, and Ezra[46] showed in a three-DOF model for intramolecular energy flow in the OCS molecule that, although the motion is chaotic, some local frequencies are often fairly constant over times corresponding to many vibrational periods when the system moves along resonance zones, and long time correlations are often observed near the junctions of resonance zones. In Fig. 7, which shows the time evolution of the second-order frequencies $\overline{\omega_k^{2\mathrm{nd}}}(\mathbf{p},\mathbf{q})$ at $E=0.5\epsilon$ for saddle I, we can see that in addition to the reactive mode frequency $\overline{\omega_1^{2\mathrm{nd}}}$, some other frequencies, e.g., $\overline{\omega_k^{2\mathrm{nd}}}(k=5,6,7,9)$, are also fairly constant through the saddle region, although the corresponding actions do not maintain constancy at all. Although we have not clarified yet what mechanism locks these frequencies, we expect that the LCPT frequency analysis will provide us with a versatile tool to analyze the resonance mechanism in chaotic motions.

3. Stochastic (=fully developed chaotic) region. The system becomes subject to considerable nonlinearities of the PES at much higher energies, and the convergence radius becomes negligibly small for the LCPT near the fixed (saddle) point for the invariant of motion associated with the reactive coordinate $\overline{q_F}$. In this energy region, no approximate invariant of motion can be expected to exist, even in the passage over the saddle between wells. The saddle-crossing dynamics is entirely stochastic, with dimensionality essentially equal to the number of degrees of freedom of the system. It may not be possible to extract a dividing surface free from barrier recrossings. To describe reaction dynamics in this region, it will probably be more convenient to go back to the conventional reaction path approach in the original configuration space $\mathbf{q}$. In such a case, the variational TST approach, to choose the dividing surface to minimize the reactive flux, becomes one reasonable means to address the problem.[48–50] At these high energies above the lowest, presumably (but not necessarily) first-rank saddle, the system trajectories may pass over higher-rank saddles of the PES. These provide us with a new, untouched, exciting problem, i.e., what is the role of resonance in the imaginary ω plane for the bifurcation? (This even arises in the degenerate bending modes for a linear transition state of a triatomic molecule.) With this, we encounter the many related open subjects incorporated into statistical theories of many-DOF systems.

In this paper, we have shown that the replacement of saddle recrossing motions by single-crossing paths removes one of the remaining ambiguities in transition-state theory, even though it is not apparent whether this can be done for very-high-energy trajectories. By formulating the transition rate in second-order LCPT coordinates, the transmission coefficient becomes unity for all energies at which the reactive degree of freedom is nearly regular in the transition state region. The LCPT analysis we developed here can not only elucidate the influence of nonlinear dynamics on the invariants of motion but also effectively extract any other decoupled ''good'' coordinates associated with local invariants of motion from the many-DOF phase space. The dividing hypersurface in the transformed space, i.e., a reaction bottleneck, is a complex, momentum-dependent function. Because

of its momentum dependence and the high degree of nonlinearity of the transformation, the dividing hypersurface is not easy to visualize. However it is possible to tabulate or graph distributions of projections of this hypersurface onto low-dimensional subspaces of the principal coordinates. Such projections reveal how the complexity of the hypersurface grows with the system's velocity across the saddle and total energy of the system.[41] Such local invariants could not be detected among chaotic motions by analyses based on largest (local) Liapunov exponents, or local K entropy. A possible way to do that might be to scrutinize a positive local Liapunov exponent ''spectrum,'' although the estimations of *local* Liapunov exponents possess their own unavoidable ambiguities for small positive terms.[43,44] The forthcoming challenging problems of this subject include the following. How does the regular zone expand in the transition state region, and how does it depend on total energy and the other physical quantities? How are the bath-DOF's resonance zones distributed,[51] and how do they influence the topologies of the local dynamics in the transition state where the system would stay only for a ''finite'' time? How could we extend the analysis to much higher-energy regions in which a few, finite order perturbative calculations would diverge rapidly and kinds of resummation methods[9,52–55] or other nonperturbative methods[46] might be desired? These are some of the subjects still to be addressed.

ACKNOWLEDGMENTS

T.K. expresses his gratitude to Professor K. Fukui (deceased), Professor. I. Ohmine, Professor M. Nagaoka, and Dr. M. Toda for their valuable suggestions and discussions, and to Dr. K.D. Ball for his computational assistance. We thank the Institute for Nuclear Theory at the University of Washington for its hospitality and the Department of Energy for partial support during the completion of this work. This study was supported by the fellowship of the Japan Society for the Promotion of Science (JSPS), and by the National Science Foundation.

[1] C. Amitrano and R. S. Berry, Phys. Rev. Lett. **68**, 729 (1992); Phys. Rev. E **47**, 3158 (1993).
[2] T. L. Beck, D. M. Leitner, and R. S. Berry, J. Chem. Phys. **89**, 1681 (1988).
[3] R. J. Hinde and R. S. Berry, J. Chem. Phys. **99**, 2942 (1993).
[4] R. S. Berry, Chem. Rev. **93**, 237 (1993).
[5] R. S. Berry, Int. J. Quantum Chem. **58**, 657 (1996).
[6] E. R. Lovejoy, S. K. Kim, and C. B. Moore, Science **256**, 1541 (1992).
[7] R. A. Marcus, Science **256**, 1523 (1992).
[8] I. Ohmine, J. Phys. Chem. **99**, 6767 (1995).
[9] R. B. Shirts and W. P. Reinhardt, J. Chem. Phys. **77**, 5204 (1982); **79**, 3173 (1983).
[10] M. J. Davis and S. K. Gray, J. Chem. Phys. **84**, 5389 (1986).
[11] S. Wiggins, *Normally Hyperbolic Invariant Manifolds in Dynamical Systems* (Springer, New York, 1991).
[12] R. E. Gillian and G. S. Ezra, J. Chem. Phys. **94**, 2648 (1991).
[13] M. Toda, Phys. Rev. Lett. **74**, 2670 (1995).
[14] M. Toda, Phys. Lett. A **227**, 232 (1997).
[15] T. Komatsuzaki and M. Nagaoka, J. Chem. Phys. **105**, 10838 (1996).
[16] T. Komatsuzaki and M. Nagaoka, Chem. Phys. Lett. **265**, 91 (1997).
[17] T. Komatsuzaki and R. S. Berry (unpublished).
[18] A. J. Lichtenberg and M. A. Lieberman, *Regular and Chaotic Dynamics*, 2nd ed. (Springer, New York, 1992).
[19] G. Hori, Publ. Astron. Soc. Jpn. **18**, 287 (1966); **19**, 229 (1967).
[20] A. Deprit, Celest. Mech. **1**, 12 (1969).
[21] A. J. Dragt and J. M. Finn, J. Math. Phys. **17**, 2215 (1976); **20**, 2649 (1979).
[22] J. R. Cary, Phys. Rep. **79**, 130 (1981).
[23] L. E. Fried and G. S. Ezra, J. Chem. Phys. **86**, 6270 (1987).
[24] L. E. Fried and G. S. Ezra, Comput. Phys. Commun. **51**, 103 (1988).
[25] L. E. Fried and G. S. Ezra, J. Phys. Chem. **92**, 3144 (1988).
[26] M. Page and J. W. McIver, Jr., J. Chem. Phys. **88**, 922 (1988).
[27] At a nonstationary point there exist only three zero-frequency modes corresponding to the total translational motions and the normal coordinates of the infinitesimal rotational motions appear in all the terms including the zeroth-order Hamiltonian.
[28] The canonical perturbation theory can be applied to some nonzero total angular momentum systems by Dragt and Finn's two-step transformation—Ref. 21 The discussions will be given elsewhere.
[29] W. H. Miller, Faraday Discuss. Chem. Soc. **62**, 40 (1977).
[30] T. Seideman and W. H. Miller, J. Chem. Phys. **95**, 1768 (1991).
[31] R. Hernandez and W. H. Miller, Chem. Phys. Lett. **214**, 129 (1993).
[32] H. Goldstein, *Classical Mechanics* (Addison–Wesley, Reading, MA, 1950).
[33] See AIP Document No. E-PAPS: EJCPSA6-110-509918 for the full expansions of the transformed coordinates and momenta, in first and second order and in both saddle regions. E-PAPS document files may be retrieved free of charge from AIP's FTP server (http://www.aip.org/pubservs/paps.html) or from ftp.aip.org in the directory /epaps/. For further information: e-mail: paps@aip.org or fax: 516-576-2223.
[34] The δ_V was determined empirically by checking whether it gives indistinguishable PES and LCPT transformations with smaller δ_V. For example, even with $\delta_V=1\times10^{-8}$, the total numbers of the three-, and four-body nonlinear couplings terms were less changed than with $\delta_V=2\times10^{-5}$, i.e., 107 and 380 for saddle I, and 189 and 700 for saddle II, respectively, the number of total terms in $\overline{H}_2$ (saddle I) is the same with $\delta_V=2\times10^{-5}$, without any significant change in coefficients with each term.
[35] J. C. Keck, Discuss. Faraday Soc. **33**, 173 (1962).
[36] J. B. Anderson, J. Chem. Phys. **58**, 4684 (1973).
[37] J. P. Bergsma, J. R. Reimers, K. R. Wilson, and J. T. Hynes, J. Chem. Phys. **85**, 5625 (1986).
[38] J. P. Bergsma, B. J. Gertner, K. R. Wilson, and J. T. Hynes, J. Chem. Phys. **86**, 1356 (1987).
[39] B. J. Gertner, K. R. Wilson, and J. T. Hynes, J. Chem. Phys. **90**, 3537 (1989).
[40] W. H. Press, S. A. Teukolsky, W. T. Vetterling, and B. P. Flannery, *Numerical Recipes*, 2nd ed. (Cambridge University Press, New York, 1992).
[41] T. Komatsuzaki and R. S. Berry, Phys. Chem. Chem. Phys. **1**, 1387 (1999).
[42] Such a characteristic time can be estimated by a plateau time τ_p; $\tau_p=1/(\kappa^{\mathrm{MD}}(0)-\kappa^{\mathrm{MD}}(\tau))\int_0^\tau dt[\kappa^{\mathrm{MD}}(t)-\kappa^{\mathrm{MD}}(\tau)]$ where τ is the simulation cutoff time in evaluating $\kappa^{\mathrm{MD}}(t)$. τ_p would be the $1/e$ relaxation time if $\kappa^{\mathrm{MD}}(t)$ were exponential (Ref. 38). The τ_p are estimated as 1.359(I), 1.322(II) (at $E=0.1\epsilon$), 1.041(I), 0.935(II) (0.5ϵ), and 1.048(I), 1.133(II) (1.0ϵ), where the number in parentheses denotes either saddle I or saddle II.
[43] D. J. Wales and R. S. Berry, J. Phys. B **24**, L351 (1991).
[44] R. J. Hinde, R. S. Berry, and D. J. Wales, J. Chem. Phys. **96**, 1376 (1992).
[45] The quantity $\omega_F(\mathbf{p},\mathbf{q})$ might not necessarily maintain its approximate invariance even while the associated action $\overline{J}_F$ does, because $\overline{\omega}_F$ depends on not only $\overline{J}_F$ but also the other $\overline{J}_k(k\neq F)$ [see Eq. (10)]. The equation of motion of the kth mode itself [Eqs. (12) and (13)] is rigorously satisfied if the $\overline{J}_k$ is conserved despite the constancy or nonconstancy of $\overline{\omega}_k(\overline{\mathbf{J}})$. As seen in Fig. 7, in almost cases in this study the frequencies $\overline{\omega}_1(\mathbf{p},\mathbf{q})$ were fairly well conserved during saddle crossings as were the actions $\overline{J}_1$. Even if it were not so, we might still expect any nonconstancy of $\overline{\omega}_F$ to leave the separability of $\overline{q}_F$ as unaffected as $\overline{J}_F$ in the transition state. The reason is that to pass through a dividing surface from one side to the other, the crossing trajectories typically require, at most, a half-period of the reactive hyperbolic orbit $\sim\pi/\overline{\omega}_F$; the fluctuation of $\overline{\omega}_F$ should have little influence during such short time intervals. We are now analyzing this in detail.
[46] C. C. Martens, M. J. Davis, and G. S. Ezra, Chem. Phys. Lett. **142**, 519 (1987).

[47] M. J. Davis, J. Chem. Phys. **83**, 1016 (1985).
[48] D. G. Truhlar, B. C. Garrett, and S. J. Kippenstein, J. Phys. Chem. **100**, 12771 (1996).
[49] D. C. Chatfield, R. S. Friedman, S. L. Mielke, G. C. Lynch, T. C. Allison, D. G. Truhlar, and D. W. Schwenke, in *Dynamics of Molecules and Chemical Reactions*, edited by R. E. Wyatt and J. Z. H. Zhang (Dekker, New York, 1996), p. 323.
[50] J. Villa and D. G. Truhlar, Theor. Chem. Acc. **97**, 317 (1997).
[51] In some trajectories at moderately high energies it was found that $\overline{H}_0(\overline{\mathbf{p}}^{2\mathrm{nd}},\overline{\mathbf{q}}^{2\mathrm{nd}})=\Sigma_{k=1}^{12}\omega_k\overline{J}_k^{2\mathrm{nd}}(\mathbf{p},\mathbf{q})$ tend to maintain an approximate constant of motion during saddle crossings in addition to $\overline{J}_1^{2\mathrm{nd}}(\mathbf{p},\mathbf{q})$. It implies that while there might not exist any approximate constant of action for each bath DOF, the system could possess an additional approximate constancy in some portions of the phase space in the transition state.
[52] G. A. Baker Jr., *Essentials of Padé Approximants* (Academic, New York, 1975).
[53] D. Farrelly and T. Uzer, J. Chem. Phys. **85**, 308 (1986).
[54] L. E. Fried and G. S. Ezra, J. Chem. Phys. **90**, 6378 (1989).
[55] As an another approach altering the zeroth-order integrable Hamiltonian, see I. D. Feranchuk and L. I. Komarov, Phys. Lett. A **88**, 211 (1982).